www.czasopisma.pan.pl PAN www.journals.pan.pl

Opto-Electronics Review 27 (2019) 268–274

Contents lists available at ScienceDirect

Opto-Electronics Review

journal homepage: http://www.journals.elsevier.com/opto-electronics review

Passive synthesis rules of coupled-cavity quantum cascade lasers

M. Krysicki *, B. Salski, P. Kopyt

Institute of Radioelectronics and Multimedia Technology, Warsaw University of Technology, ul. Nowowiejska 15/19, 00-665 Warsaw, Poland

ARTICLE INFO

Article history:
Received 11 September 2018
Received in revised form 29 July 2019
Accepted 7 August 2019
Available online 10 September 2019

Keywords:
Quantum cascade lasers
Coupled cavities
Resonance characterization
Threshold gain
Lasers

ABSTRACT

A new approach to passive electromagnetic modelling of coupled–cavity quantum cascade lasers is presented in this paper. One of challenges in the rigorous analysis of such eigenvalue problem is its large size as compared to wavelength and a high quality factor, which prompts for substantial computational efforts. For those reasons, it is proposed in this paper to consider such a coupled-cavity Fabry-Perot resonant structure with partially transparent mirrors as a two-port network, which can be considered as a deterministic problem. Thanks to such a novel approach, passive analysis of an electrically long laser can be split into a cascade of relatively short sections having low quality factor, thus, substantially speeding up rigorous electromagnetic analysis of the whole quantum cascade laser. The proposed method allows to determine unequivocally resonant frequencies of the structure and the corresponding spectrum of a threshold gain. Eventually, the proposed method is used to elaborate basic synthesis rules of coupled–cavity quantum cascade lasers.

Introduction

The idea of semiconductor lasers with a single edge-emitting cavity split in two cavities coupled via an air gap was first demonstrated in Ref. 1. One of major advantages of such splitting is in the possibility to suppress the whole bunch of spurious modes occurring within a broad gain spectrum of an active medium and maintaining only selected longitudinal mode of interest. That kind of splitting can be easily made in a single bulk cavity with reactive ion etching [2] or focused ion beam [3]. Since the first demonstration of cavity splitting, a lot of research has been undertaken to study experimentally the impact of coupled cavities on the performance of various kinds of lasers [4–6]. One of specific applications are quantum cascade lasers (QCLs), which are usually in the form of an edge-emitting Fabry-Perot (FP) cavity with an active heterostructure made of a stack of semiconductor multiple quantum wells. QCLs operate either in the infrared or terahertz spectral range [7], although the latter one still requires cryogenic temperatures to achieve stable generation [8]. However, despite obvious advantages of using coupled FP cavities, only a little effort has been undertaken, so far, to elaborate systematically the analysis and synthesis rules of such structures, which in turn hardens the efforts toward establishing common design rules.

For those reasons, the aim of this paper is to propose a general approach to the analysis of coupled FP cavities, which will then be used to elaborate basic synthesis rules. Section 2 shows novel methodology for electromagnetic analysis of coupled FP cavities, while Section 3 addresses major properties of coupled FP cavities, which have the influence on spectral characterization of the longitudinal modes. It is assumed without loss of generality that the QCL operates in the infrared spectrum.

Electromagnetic analysis of coupled cavities

It has been shown in Ref. 9 that resonant frequencies of a single section of a FP cavity of the length L can be uniquely determined from the following measure resulting from the summation of a discrete series of an infinite number of reflections of electromagnetic (EM) wave from mirrors terminating the cavity:

$$A = 1 - r_1 r_2 e^{-\gamma 2L}, \tag{1}$$

where r_1 (r_2) stands for the reflectivity of the left (right) mirror, and γ is the complex propagation factor.

That concept has been extended in Ref. 10 where the authors have shown that a can be calculated by splitting resonant cavity into two non-resonating sections, as shown in Fig. 1, and calculating reflection coefficients of each section of the divided cavity:

$$A = E_f^{-1} = 1 - S_{11L} S_{11R}, \tag{2}$$

where E_f represents the forward-propagating wave inside the cavity, and S_{11L}, S_{11R} are the reflection coefficients of the left- and

* Corresponding author.
E-mail address: mkrysicki@ire.pw.edu.pl (M. Krysicki).

https://doi.org/10.1016/j.opelre.2019.08.001
1230-3402/

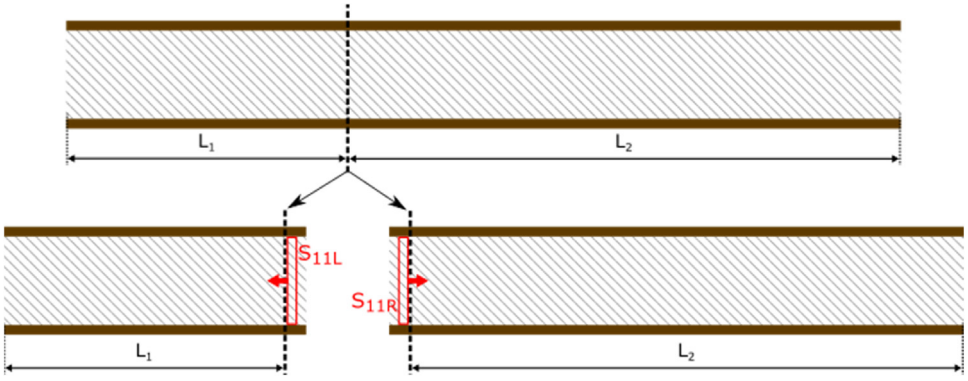

Fig. 1. Longitudinal cross-section of a single section of an FP cavity built of a metal-metal waveguide terminated with etched planes divided for computational reasons into two low Q-factor sections which can be analyzed separately for complex reflection coefficients: S_{11L} and S_{11R}.

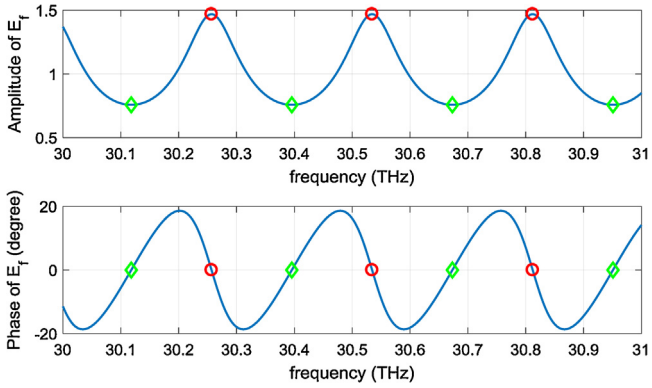

Fig. 2. Magnitude (top) and phase (bottom) of the forward-propagating wave E_f as a function of frequency computed for a single GaAs block ($n = 3.6$) of length $L = 150$ μm terminated with air ($n = 1$). Resonances (anti-resonances) are indicated with green (red) markers.

right-hand side section of the structure, respectively. In principle, it means that the eigenvalue resonant problem can be split into two deterministic non-resonant problems with a much lower quality factor (Q-factor). This is of crucial importance if, for some reason, time-domain numerical methods, which are not well suited to the analysis of structures exhibiting a high Q-factor due to prohibitively long computing time, are supposed to be used in the EM analysis.

According to Ref. 10, two conditions must be met at resonance, namely, the minimum of the magnitude $|E_f|$ and zero of the phase $\angle E_f$. That property can be shown on a simple one-dimensional example consisting of a single block of lossless GaAs dielectric ($n = 3.6$) of length $L = 150\,\mu m$ terminated with air ($n = 1$). It can be expected that resonances, corresponding to consecutive multiples of the half of the wavelength between the mirrors, will occur at:

$$f = N\frac{c}{2Ln}, \tag{3}$$

where $N = 1,2,3,\ldots$, c is the speed of light, and n is the refractive index of GaAs. To confirm that, the structure was split into two equal sections and, subsequently, the corresponding reflection coefficients were calculated using a transfer–matrix method [11]. Spectral characteristics of the forward-propagating wave obtained with Eq. (1) is shown in Fig. 2, which indicates that a good agreement with theoretical resonant frequencies, as given in Eq. (3), has been obtained.

Unfortunately, the aforementioned splitting method is unequivocal only for structures consisting of a single homogeneous resonant section. In case of coupled cavities [12,13], the global measure of the forward-propagating wave E_f becomes ambiguous, as in fact each cavity section contains different forward- and backward-propagating waves. Figure 3 shows the view of an exemplary structure consisting of three GaAs blocks ($n = 3.6$), each of length $L = 50$ μm, separated by two 2.5 μm long air gaps ($n = 1$). The structure has been split at three different planes: in the middle of the first dielectric slab, in the middle of the second dielectric slab and in the middle of the first air gap. As it can be noticed in Fig. 4, the frequency of anti-resonances, corresponding to the maximum

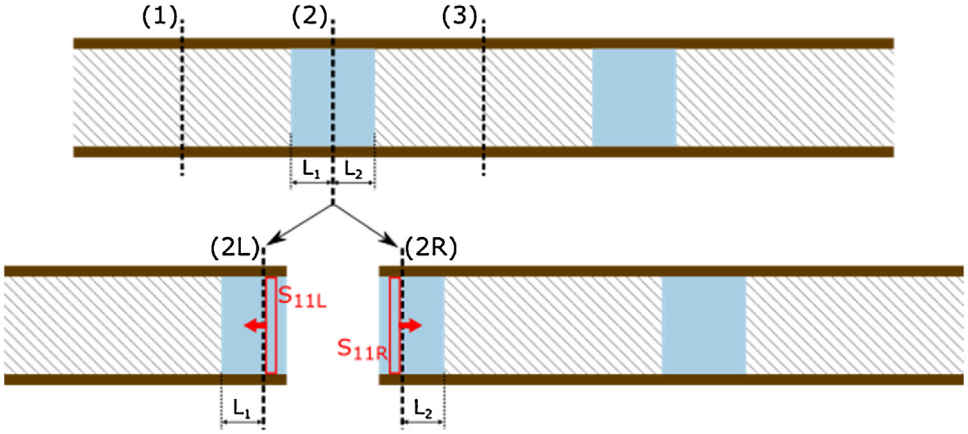

Fig. 3. Three GaAs blocks (grey area), each of length $L = 50$ μm, separated by two 2.5 μm long air gaps (blue area). The structure has been split at three different planes: in the middle of the first dielectric slab (plane 1), in the middle of the second dielectric slab (plane 3) and in the middle of the first air gap (plane 2), for which the splitting method is presented.

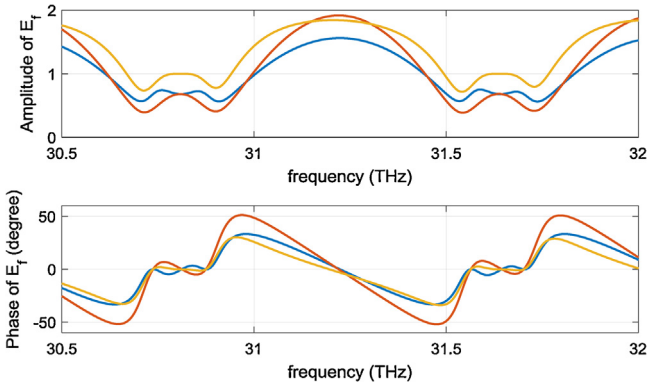

Fig. 4. Magnitude (top) and phase (bottom) of the forward-propagating wave E_f as a function of frequency computed for three GaAs blocks, each of length L = 50 μm, separated by two 2.5 μm long air gaps. The structure has been split at three different planes (see Fig. 3): in the middle of the first dielectric slab (blue line), in the middle of the second dielectric slab (red) and in the middle of the first air gap (orange line).

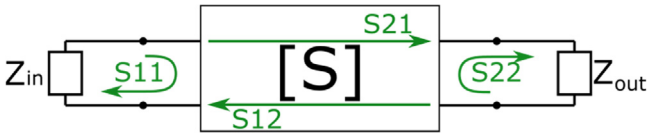

Fig. 5. Two-port network representation of a FP cavity.

of $|E_f|$, seems to be uniquely determined, although the shape of the function is varying. On the contrary, the position of resonances substantially depends on the splitting plane, thus, making the method hardly useful in spectral analysis of coupled cavities.

For that reason, an alternative novel approach is proposed in this paper to the analysis of coupled cavities, which lacks drawbacks of the splitting approach. The formulation of the new approach starts from reciprocity theorem [14], which states that spectral and angular properties of any radiating structure (or transmitter) are kept unchanged if that structure is considered as termination (or receiver). As a result, the laser embedded in an FP resonant structure, which is radiating EM field outside the cavity through both mirrors, like the QCL with coupled cavities, can be considered as a two-port network driven with the signal at one port and terminated on the other side. Such a network can be represented with the scattering matrix [S] as shown in Fig. 5.

Let us consider at first the choice of input and output impedances in the model shown in Fig. 5. Since in radiation regime, the cavity is loaded at both sides with radiation impedance representing partial leakage of energy generated inside the cavity, it is straightforward to apply exactly the same termination impedances at both ends of the two-port network. Spectral characteristics of radiation impedance can be computed rigorously using full-wave electromagnetic modelling tools based on such numerical methods as finite-difference time-domain (FDTD) [15,16]. Consider, for example, a transverse electromagnetic mode propagating along one of external GaAs coupled cavities, as shown in Fig. 3, which is open to the free space. If the height of the GaAs block is 8 μm, as in Ref. 1, radiation impedance will be equal to $Z_{in} = Z_{out} = 369.8677 - j19.11419\ \Omega$ in the 30 THz – 33 THz frequency range.

Figure 6 shows a transmission coefficient S_{21}, computed for coupled cavities discussed earlier (compare Fig. 3) assuming that the structure is terminated with $Z_{in} = Z_{out} = 120\pi\ \Omega$ (see blue line) and, subsequently, with the already calculated complex radiation impedance (see orange line). Unlike in the splitting method (compare Fig. 4), the maximum of $|S_{21}|$ corresponds uniquely to the resonant frequencies of the structure.

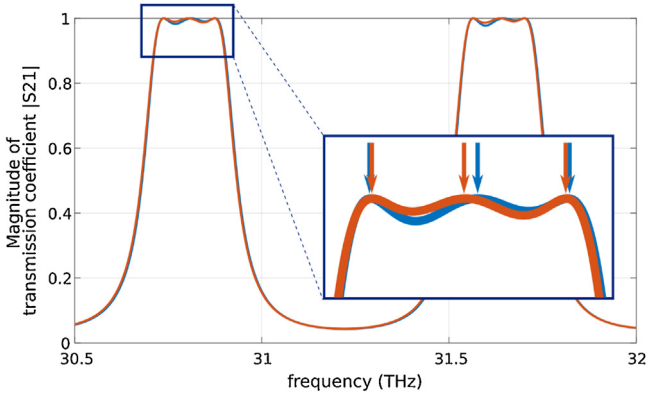

Fig. 6. Magnitude of a transmission coefficient of three GaAs blocks, each of length L = 50 μm, separated by two 2.5 μm long air gaps surrounded by air located in a parallel plate line (blue line) or surrounded by unbounded free space (red line). Resonances are indicated with arrows.

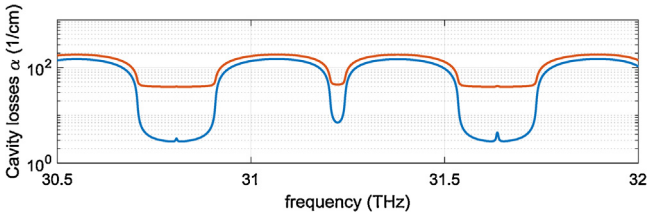

Fig. 7. Cavity losses (blue line) and threshold gain (red line) computed for three GaAs blocks $n = 3.6$, $\sigma = 3\,S/m$), each of length L = 50 μm, separated by two 2.5 μm long air gaps.

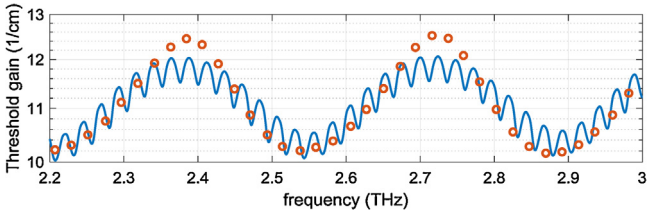

Fig. 8. Gain threshold computed with the algorithm proposed in this paper (solid line) compared with Ref. [19] (dots). Computed geometry consists of two GaAs active region blocks (1800 μm and 125 μm long) separated bya 4 μm-long air gap placed on a thin (300 nm) $Al_{0.5}Ga_{0.5}As$ layer and a semi-insulating GaAs substrate.

Another important parameter of coupled FP cavities that needs to be addressed is a threshold gain defined as:

$$g_{th}(f) = \frac{\alpha_0 - \frac{1}{2L}\ln(r_1 r_2)}{\Gamma}, \tag{4}$$

where α_0 represents the effective losses inside a cavity and Γ is the confinement factor. Effective losses of the cavity can be obtained from the previously computed scattering matrix [S] using Nicolson – Ross – Weir algorithm [17,18], which allows to extract complex refractive index of effective medium from [S] parameters representing the whole cavity. Let us consider again the example of coupled cavities shown in Fig. 3 but with additional medium losses, for example: $\sigma = 3\,S/m$. The resulting cavity losses and a threshold gain, assuming that $\Gamma = 1$ (all EM field is contained within the active medium), are presented in Fig. 7. It can be noticed that the minimum threshold gain corresponds to the maximum of transmission shown in Fig. 6 achieved at resonance. A smaller and much narrower local dip in the threshold gain has been also achieved at anti-resonances, where the transmission through the cavity is at the minimum.

Figure 8 shows comparison between gain threshold computed using the approach proposed in this paper (blue line) as compared

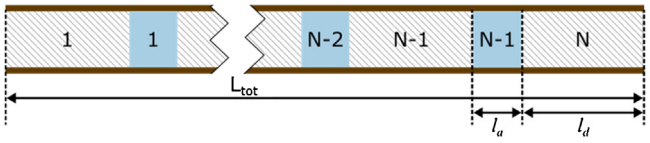

Fig. 9. Coupled cavities consisting of N GaAs blocks separated by N-1 air gaps.

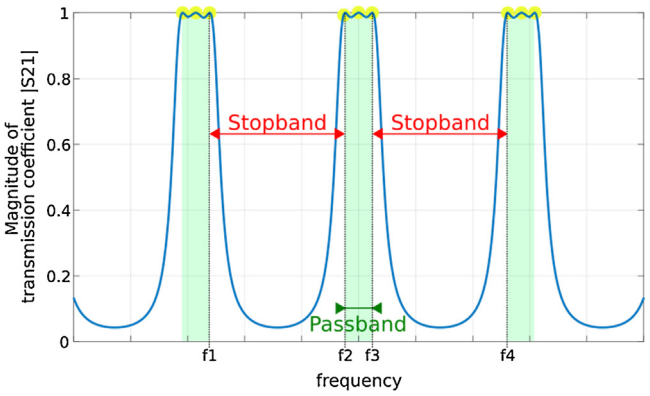

Fig. 10. Typical spectrum of the magnitude of a transmission coefficient, $|S_{21}|$, of the structure presented in Fig. 9.

with the alternative approach [19] (orange dots). The geometry under study consists of two GaAs active region blocks (1800 μm and 125 μm long) separated by the 4μm-long air gap and placed on a thin (300 nm) $Al_{0.5}Ga_{0.5}As$ layer deposited on a semi-insulating GaAs substrate. First of all, it can be noticed that periodicity of the characteristics is very similar. However, the method proposed in this paper accounts also for a multipath effect contributing to the presence of the periodic ripples visible in the characteristics. Period of those ripples is equal to 24 GHz and corresponds with length of half-wavelength in longer active region block.

In conclusion of this Section, the method applicable to the analysis of coupled FP cavities has been proposed and validated on simple examples. The method takes the advantage of the fact that the FP cavity can be represented as a two-port network using the scattering matrix [S]. It has been shown that the proposed method allows to unequivocally derive basic properties of the coupled cavities, like the spectrum of a threshold gain. Such an approach to the analysis of coupled FP cavities has never been proposed before. In the next Section, the proposed analysis method will be applied to elaborate the synthesis procedure of a Fabry-Perot QCL consisting of coupled cavities.

Electromagnetic synthesis of coupled cavities

As it has been shown in Ref. [19], spectral shape of total losses of the QCL composed of two coupled cavities separated by an air gap varies substantially with geometry. However, there are still lacking specific synthesis rules that would enable realization of the QCL coupled cavities with a priori specified characteristics. Therefore, a new methodology for design of such coupled structures will be presented in this Section.

Let us assume that the geometry consists of *N* GaAs blocks separated by *N-1* air gaps, as presented in Fig. 9. A typical spectrum of the magnitude of a transmission coefficient $|S_{21}|$ of such structure is shown in Fig. 10. With analogy to RF filter design rules, periodically repeated bands with a high transmission level are called *passbands*, while the portion of the spectrum with low transmission is called *stopband*, although such notions are not commonly used if a cavity is considered from its inside, where laser generation takes place in the middle of the passband. In general, the number of poles in the

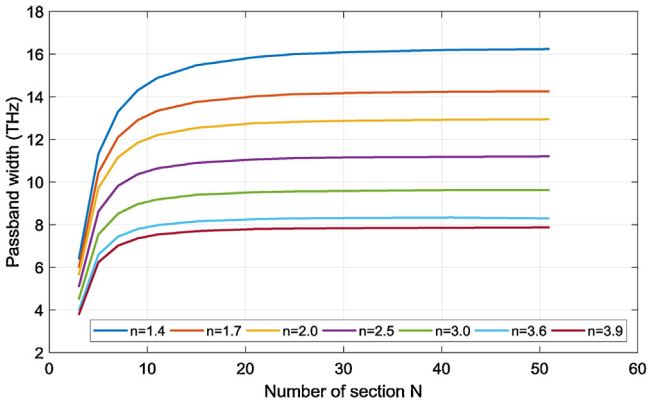

Fig. 11. Passband width as a function of the number of dielectric sections *N* calculated for various refractive indices.

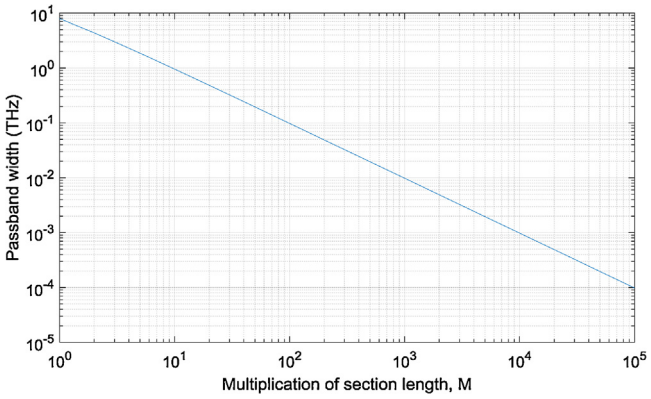

Fig. 12. Passband width as a function of the length of dielectric sections normalized to the half of the wavelength.

passband is associated with the number of coupled cavities. Lengths of air gap (l_a) and dielectric (l_d) sections depend on the expected position of the passband and can be determined using following formulas:

$$l_a = (2P+1)\frac{\lambda_0}{4} = (2P+1)\frac{c}{4f_0} \tag{5}$$

$$l_d = M\frac{\lambda}{2} = M\frac{c}{2nf_0}, \tag{6}$$

where f_0 is the center frequency of the passband calculated as the arithmetical mean of f_2 and f_3 indicated in Fig. 10, and *M* and *P* are natural numbers. As it can be noticed, the length of dielectric sections should be equal to the multiple of the half of the wavelength, while air gap sections should function as impedance inverters, so their length is quarter of the wavelength (or its odd multiple) [20].

Subsequently, the relation between the number of dielectric sections *N* and a passband width has been evaluated for various values of the refractive index of dielectric material (see Fig. 11). It can be noticed that the passband generally increases with *N* and converges for relatively large *N*. Convergence of the passband width occurs faster with *N* if the contrast between refractive indices of the dielectric section and the gap becomes larger. Moreover, the largest passband width can be obtained if the refractive index contrast is smaller. Similar behaviour can be observed for the stopband.

Next, Figure 12 shows the impact of the length of dielectric sections normalized to the half of the wavelength (*M*) on the passband width, assuming that $N = 10$ and $n = 3.6$. The number of dielectric sections (*N*) is large enough to assume that the passband only little depends on *N* (compare Fig. 11). Consequently, it can be concluded

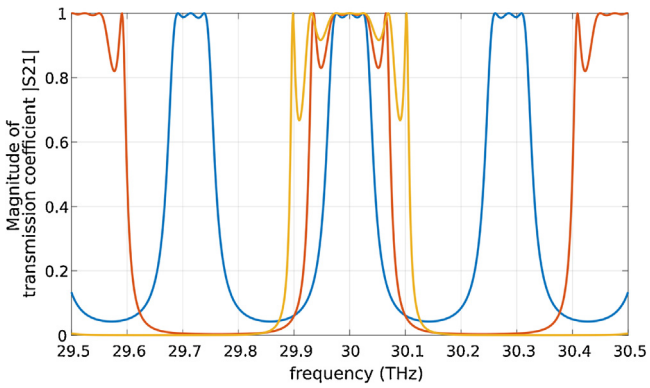

Fig. 13. Transmission through 3 GaAs blocks, each of length $L = 145.732$ μm (blue line), 5 GaAs blocks, each of length $L = 87.439$ μm (red line) and 7 GaAs blocks, each of length $L = 62.457$ μm (orange line), separated by two 2.5 μm long air gaps. In each case, the total length of the laser is assumed as $L_{tot} = 0.5$ mm.

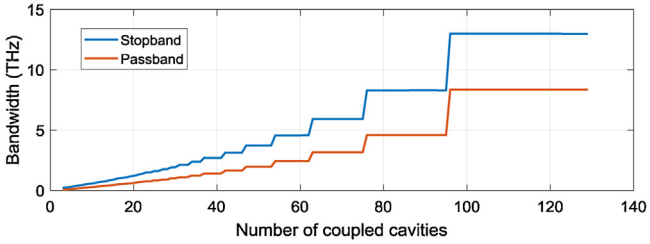

Fig. 14. Stopband (blue line) and passband (orange line) widths as a function of the number of equally long dielectric sections, assuming that the total length of the laser should be approximately equal to $L_{tot} = 0.5$ mm.

from Fig. 12 that the passband decreases logarithmically with M, as could be expected.

If N is large enough so that the passband width no longer depends on N (see Fig. 11), the air gap length multiplication factor M can be estimated upon required spectral data in the following way:

$$P = \frac{1}{2}\left(\frac{f_0}{f_3 - f_2} - 1\right). \tag{7}$$

Practically, it means that one can narrow spectral width of a reduced threshold gain, $\Delta f = f_3 - f_2$, centred at f_0, at the expense of the increased electric length of dielectric sections. However, the scale of reduction of the spectral width of a low-threshold gain is limited as the distance between consecutive passbands is equal to $\frac{f_0}{2P+1}$, which should be much larger than a relatively broad spectral width of gain of the active medium to avoid laser generation at frequencies other than f_0.

In practice, it is quite common that the total length of the laser is roughly imposed by manufacturing technology. In that case, there is limited freedom of choice of the number of coupled sections that will satisfy the aforementioned length-to-wavelength rules. Assuming that the total length of all dielectric sections is imposed, the increase of the number of coupled cavities results in the decrease of their individual lengths and, consequently, in the increase of the passband and stopband widths (see Fig. 13).

In Fig. 14, the width of stop- and pass-bands as a function of the number of equally long sections is shown, assuming that the total length of the laser should be approximately equal to $L_{\text{tot}} = 0.5$ mm. It can be noticed that both bandwidths are almost linearly increasing with the number of coupled cavities N, provided that N is relatively small, which is in agreement with Fig. 11. At some point, however, further increase of N no longer shapes the bandwidth and the only reason for step changes of the bandwidth is the need to further decrease the normalized length of cavities M in order to keep the total length fixed.

In real scenarios, which will be addressed in the next Section, the minimum number N of coupled laser sections has to be established to meet the requirements for the spectral shape of a gain threshold.

Table 1
QCL stack as presented in Ref. 7.

Material	Height [μm]	Doping n $\left[cm^{-3}\right]$
GaAs	1	$6 \cdot 10^{18}$
GaAs	3.5	$4 \cdot 10^{16}$
Active region	1.62	
GaAs	3.5	$4 \cdot 10^{16}$
GaAs	1	$6 \cdot 10^{18}$
GaAs	1	$2 \cdot 10^{18}$
GaAs	450	$2 \cdot 10^{18}$

Table 2
Materials parameters as presented in Refs. 21 and 22.

Material	n $\left[cm^{-3}\right]$	τ [ps]	ε_{core}	f_{pl} [THz]	f_c [THz]
GaAs	4×10^{16}	0.5	12.4	6.9375	2
GaAs	6×10^{18}	0.1	12.4	84.9669	10
GaAs	2×10^{18}	0.1	12.4	49.0557	10

Example

A QCL made in the form of a double-plasmon Al-free GaAs waveguide for planar optical confinement will be considered in this Section. An active region consists of 36 sequences of an injector and 3 quantum-well segments. Geometrical properties of the considered stack [7] are presented in Table 1.

EM modelling of a QCL can be undertaken in two steps. At first, the parameters of the propagating mode, such as confinement factor and effective permittivity, should be determined at the cross-section of the structure and, subsequently, one dimensional simulation can be executed to consider the propagation of a given mode along the laser in order to establish spectrum of a gain threshold.

Effective parameters of the QCL structure

Material properties of the exemplary QCL geometry [7] are presented in Table 2. In the mid-infrared, GaAs semiconductor can be described with a Drude model:

$$\varepsilon(\omega) = \varepsilon_{core}(\omega) + i\frac{n e^2 \tau}{\omega m^*(1 - i\omega\tau)} = \varepsilon_{core} - \frac{\omega_{pl}^2}{\omega^2 + i\omega\Gamma}, \tag{8}$$

where ε_{core} is the relative permittivity at infinite frequency, $\omega = 2\pi f$ *is* the angular frequency, n is the semiconductor doping level, τ is the relaxation time, m^* is the effective mass of electron, $\omega_{pl} = 2\pi f_{pl}$ is the plasma angular frequency and $\Gamma = 2\pi f_c$ is the collision angular frequency.

Effective properties of a TM_{00} mode propagating in the presented geometry computed with FDTD at $f = 31$ THz ($\lambda_0 = 9.68$ μm) is $n = 3.551 + j2.27 \times 10^{-4}$, confinement factor $\Gamma = 21.81\%$, confinement loss $L = 6.73 \frac{dB}{cm}$ and effective dielectric loss $\tan\delta = 1.238 \times 10^{-4}$.

Design of QCL coupled cavities

Subsequently, the cavity is split into coupled sections in order to shape the threshold gain according to the requirements presented in Table 3.

Table 3
Design parameters used in the presented example.

Maximum total length	L_{tot} = 0.25 mm
Passband	31.35 - 31.65 THz
Stopbands	31.00 - 31.35 and 31.65 - 32.00 THz

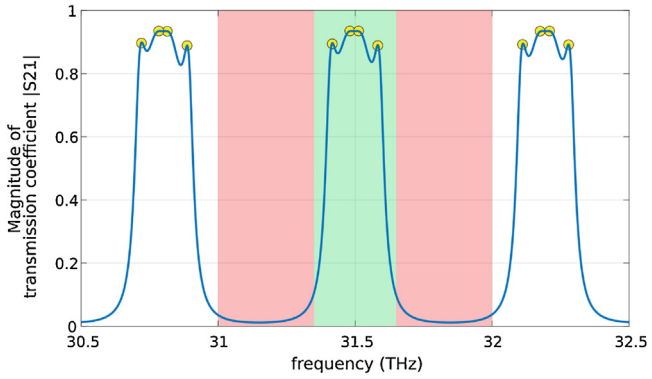

Fig. 15. Transmission (blue line) of a TM_{00} mode through four GaAs sections, each of length L = 60.31 μm, separated by 2.38 μm long air gaps. Resonant poles within passband of coupled cavities are marked with yellow circles. Green (red) areas are required passband (stopband) widths.

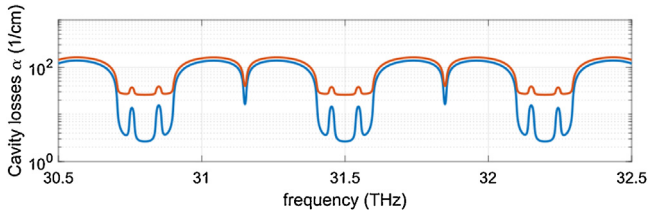

Fig. 16. Cavity losses (blue line) and threshold gain (red line) computed for three GaAs blocks ($n = 3.6$, $\sigma = 3\,S/m$), each of length L = 50 μm, separated by two 2.5 μm long air gaps.

Radiation impedance terminating the QCL open to the free space, as computed with FDTD, is equal to $Z = 399.4 - j19.97\ \Omega$. Maximum number of coupled half wavelength dielectric slabs at the centre frequency f_0 was calculated to be $Nmax = 67$. Next, the minimum order $Nmin = 4$ of such filter that still meets design requirements was found using a bi-section algorithm. Eventually, length of each dielectric section (air gap) is L = 60.31 μm (2.38 μm), which leads to the total length of the cavity equal to 248.38 μm, was established. Results are presented in Figs. 15 and 16. It can be noticed that design requirements, indicated with shaded regions in Fig. 15, are well satisfied which results in a decrease of effective cavity losses by over one order of magnitude at the frequency of laser generation.

Conclusions

In conclusion, a new approach to the analysis of coupled Fabry-Perot cavities has been demonstrated. It has been shown that a resonant structure with partially transparent mirrors can be considered as a two-port filter network fed from and terminated with radiation impedance. The method allows to determine unequivocally resonant frequencies of the structure and the corresponding spectrum of a threshold gain. These figures of merit are computed in this paper using a widely known transfer matrix method. The advantage is that instead of solving an eigenvalue problem, which is often cumbersome and may require dedicated solvers based on, e.g., mode-matching techniques, the proposed method is fully deterministic and can be split into several low-quality-factor problems.

Subsequently, essential properties of coupled Fabry–Perot cavities have been presented. First of all, it has been shown that the length of air gaps should be odd multiple of the quarter of the wavelength long so they can operate as impedance inverters known in filter synthesis rules. Simultaneously, the length of dielectric sections should be multiple of the half of the wavelength to become transparent from the impedance transformation point of view. Secondly, it has been shown that over a dozen of dielectric sections is usually enough to extend spectrum of the low-threshold gain to the maximum available for given refractive index of the dielectric section. The maximum bandwidth can be narrowed if higher refractive index is applied. However, the total number of dielectric sections should not be too large to avoid unwanted broadening of the low-threshold gain spectrum width. Practically, the spectrum of the low-threshold gain can be easily adjusted in a broad range by changing the length of the air gaps.

CRediT authorship contribution statement

M. Krysicki: Conceptualization, Data curation, Methodology, Resources, Software, Writing - original draft, Writing - review & editing. **B. Salski:** Conceptualization, Methodology, Project administration, Resources, Supervision, Validation, Writing - review & editing. **P. Kopyt:** Conceptualization, Investigation, Project administration, Resources, Validation, Writing - review & editing.

Acknowledgement

This work was partially supported by the Polish National Science Center within the SONATA project titled “Full-wave electromagnetic modelling of coherent radiation in electrically-pumped metal-clad semiconductor lasers with a folded cavity” (UMO-2014/15/D/ST7/05221).

References

[1] L.A. Coldren, K.J. Ebeling, J.A. Rentschler, C.A. Burrus, D.P. Wilt, Continuous operation of monolithic dynamic-single-mode coupled-cavity lasers, Appl. Phys. Lett. 44 (1984) 368–370, http://dx.doi.org/10.1063/1.94771.
[2] N. Roxhed, P. Griss, G. Stemme, Tapered deep reactive ion etching: method and characterization, TRANSDUCERS 2007 - 2007 International Solid-State Sensors, Actuators and Microsystems Conference (2007) 493–496, http://dx.doi.org/10.1109/SENSOR.2007.4300175.
[3] S.- Kim, T. Yamashita, K.- Lee, M. Nagao, M. Sato, H. Maeda, Development of 3-D focused-ion-beam (FIB) etching methods for nano- and micro-technology application, Digest of Papers. Microprocesses and Nanotechnology 2001. 2001 International Microprocesses and Nanotechnology Conference (IEEE Cat. No.01EX468) (2001) 34–35, http://dx.doi.org/10.1109/IMNC.2001.984055.
[4] H. Ibrahim, M. Ahmed, F. Koyama, Large signal modultion analysis of high-speed transverse coupled cavity VCSELs, 2017 Conference on Lasers and Electro-Optics (CLEO) (2017) 1–2, http://dx.doi.org/10.1109/CLEOPR.2017.8119069.
[5] S. Arafin, G. Morrison, M. Mashanovitch, L.A. Johansson, L.A. Coldren, Coupled-cavity lasers for a low-power integrated coherent optical receiver, 2017 Conference on Lasers and Electro-Optics (CLEO) (2017) 1–2.
[6] P. Fuchs, J. Seufert, J. Koeth, J. Semmel, S. Höfling, L. Worschech, A. Forchel, Widely tunable quantum cascade lasers with coupled cavities for gas detection, Appl. Phys. Lett. 97 (2010), 181111, http://dx.doi.org/10.1063/1.3514247.
[7] M. Bugajski, K. Kosiel, A. Szerling, J. Kubacka-Traczyk, I. Sankowska, P. Karbownik, A. Trajnerowicz, E. Pruszyńska-Karbownik, K. Pierściński, D. Pierścińska, GaAs/AlGaAs (∼ 9.4 μm) quantum cascade lasers operating at 260 K, Bull. Polish Acad. Sci. Tech. Sci. 58 (2010) 471–476, http://dx.doi.org/10.2478/v10175-010-0045-z.
[8] B.S. Williams, S. Kumar, Q. Hu, J.L. Reno, High-power terahertz quantum-cascade lasers, Electron. Lett. 42 (2006) 89–91, http://dx.doi.org/10.1049/el:20063921.
[9] L. Coldren, S. Corzine, M. Mashanovitch, Diode Lasers and Photonic Integrated Circuits, 2nd Edition, Wiley.Com. (n.d.). https://www.wiley.com/en-us/Diode+Lasers+and+Photonic+Integrated+Circuits%2C+2nd+Edition-p-9780470484128 (Accessed 13 September 2018).
[10] P. Kopyt, B. Salski, M. Sakowicz, Efficient three-dimensional electromagnetic modeling of metal–metal waveguides employed for quantum cascade lasers operating in the THz band, J. Lightwave Technol. 36 (2018) 1721–1729, http://dx.doi.org/10.1109/JLT.2018.2789584.

[11] C. Katsidis, D.I. Siapkas, General transfer-matrix method for optical multilayer systems with coherent, partially coherent, and incoherent interference, Appl. Opt. 41 (2002) 3978–3987, http://dx.doi.org/10.1364/AO.41.003978.
[12] K.J. Ebeling, L.A. Coldren, Analysis of multielement semiconductor lasers, J. Appl. Phys. 54 (1983) 2962–2969, http://dx.doi.org/10.1063/1.332498.
[13] L. Coldren, T. Koch, Analysis and design of coupled-cavity lasers - Part I: threshold gain analysis and design guidelines, IEEE J. Quantum Electron. 20 (1984) 659–670, http://dx.doi.org/10.1109/JQE.1984.1072438.
[14] C.A. Balanis, Antenna Theory: Analysis and Design, John Wiley & Sons, 2005.
[15] A. Taflove, S.C. Hagness, Computational Electrodynamics: the Finite-difference Time-domain Method, 3rd ed, Artech House, Boston, MA, 2005.
[16] W. Gwarek, M. Celuch, A. Więckowski, M. Sypniewski, Quickwave User Manuals, 1997–2017, (n.d.). http://www.qwed.eu.
[17] A.M. Nicolson, G.F. Ross, Measurement of the intrinsic properties of materials by time-domain techniques, IEEE Trans. Instrum. Meas. 19 (1970) 377–382, http://dx.doi.org/10.1109/TIM.1970.4313932.
[18] W.B. Weir, Automatic measurement of complex dielectric constant and permeability at microwave frequencies, Proc. IEEE 62 (1974) 33–36, http://dx.doi.org/10.1109/PROC.1974.9382.
[19] H. Li, J.M. Manceau, A. Andronico, V. Jagtap, C. Sirtori, L.H. Li, E.H. Linfield, A.G. Davies, S. Barbieri, Coupled-cavity terahertz quantum cascade lasers for single mode operation, Appl. Phys. Lett. 104 (2014), 241102, http://dx.doi.org/10.1063/1.4884056.
[20] G.L. Matthaei, B. Schiffman, E. Cristal, L. Robinson, Microwave Filters and Coupling Structures, Stanford Research Inst, Menlo Park CA, 1963.
[21] R. Sachs, H. Roskos, Mode calculations for a terahertz quantum cascade laser, Opt. Express 12 (2004) 2062–2069.
[22] S. Kohen, B.S. Williams, Q. Hu, Electromagnetic modeling of terahertz quantum cascade laser waveguides and resonators, J. Appl. Phys. 97 (2005), 053106.